Title

Ballistic rectification of vortex domain wall chirality at nanowire corners

Journal

Applied Physics Letters, 107(22)

ISSN

0003-6951

Authors

Omari, K

Bradley, RC

Broomhall, TJ

et al.

Publication Date

2015-11-30

DOI

10.1063/1.4936565

Ballistic Rectification of Vortex Domain Wall Chirality at Nanowire Corners

K. Omari[1], R. Bradley[1], T.J. Broomhall[1], M.P.P. Hodges[1], M.C. Rosamond[2], M.-Y. Im[3,4], P. Fischer[3,5] and T.J. Hayward[1]

[1]*Department of Materials Science and Engineering, University of Sheffield*

[2]*School of Electronic and Electrical Engineering, University of Leeds*

[3]*Centre for X-ray Optics, Lawrence Berkley National Laboratory*

[5]*Daegu Gyeongbuk Institute of Science and Technology, Daegu 711-873, Korea*

[6]*Department of Physics, University of California, Santa Cruz, California 94056, USA*

The interactions of vortex domain walls with corners in planar magnetic nanowires are probed using magnetic X-ray transmission microscopy. We demonstrate that when the domain walls are propagated into tight corners using applied fields above a critical value their chiralities are to rectified to either clockwise or anticlockwise circulation depending on whether the corners turn left or right. Single-shot focused magneto-optic Kerr effect measurements are then used to show how, when combined with modes of domain propagation that conserve vortex chirality, this allows us to dramatically reduce the stochasticity of domain pinning at artificial defect sites. Our results provide a tool for controlling domain wall chirality and pinning behaviour both in further experimental studies and in future domain wall-based memory, logic and sensor technologies.

Devices based on the controlled motion of 180° domain walls (DWs) in magnetic nanowires have been in development for over a decade [1-3]. While simple descriptions visualise DWs as rigid particles, it is well known that DWs actually have complex internal magnetisation structures [4] that change dynamically as they propagate [5-7]. Key to understanding DW structure is the concept of chirality, which describes the sense in which the magnetisation rotates across the DW. For example, in the case of vortex DWs (VDWs), which are formed in thick nanowires [4], the chirality dictates whether their internal magnetisation rotates clockwise (CW) or anticlockwise (ACW) around the out-of-plane core at the centre of the VDW.

Chirality has been shown to have a strong influence on DW behaviour. For example, VDWs with CW and ACW chirality pin differently at notches, resulting in stochastic depinning field distributions in systems where chirality is ill-defined [8,9]. Furthermore, DW chirality dictates the paths of DWs in branched nanowires, and therefore the geometry of Dirac strings in Kagome artificial spin-ice lattices [10]. In systems where DW structure can

be stabilised chirality also offers a binary degree of freedom that could be used to store information, leading to proposals for chirality-based logic networks [11].

DWs injected using conventional injection pads or current lines have random chiralities, potentially leading to uncontrolled propagation and pinning behaviours. However, by breaking symmetry, either though creating asymmetric pads [12] or by adding notches under current lines [10], chirality can be controlled at the point of injection. Controlling and manipulating chiralities during propagation is more challenging, but can be achieved by interacting DWs with asymmetrical features, such as orthogonal nanowire sections [13], large notches [14] or nanowire end-domains [15], however these approaches all involve the introduction of large defects into the nanowires. Pulsed rotating fields can be used to select DW chirality in closed ring-shaped nanowires [16], but this approach would be complex to implement in devices.

In this paper we propose a simple and effective method of controlling DW chirality in continuous nanowires. We show that DWs propagated ballistically into tight nanowire corners are reliably rectified to either CW or ACW chirality depending on whether the corner turns left or right. We then go on to show how this approach can be combined with modes of DW propagation that conserve vortex chirality to dramatically reduce the stochasticity of pinning at artificial defect sites.

To probe the interaction of VDWs with corners we fabricated 400 nm wide nanowires, with geometries similar to that shown in Fig. 1(a), on SiN_2 membranes using electron beam lithography with lift-off processing. Metallization with 40 nm of $Ni_{80}Fe_{20}$ was achieved by thermal evaporation. DWs were injected from the large pads at the nanowires' left ends and propagated into corners with radii, r = 1 μm, 2 μm or 5 μm at the right end using externally applied fields. Nanowires with corners that turned both left (UP geometry) and right (DOWN geometry) were investigated. In some nanowires a symmetrical double-notch with gap-size "g" was positioned before the corner in order to allow the chirality of the DWs to be probed prior to their interaction with the corners.

To measure the VDWs' chiralities we performed magnetic transmission soft X-ray microscopy (MTXM) using beamline 6.1.2 of the Advanced Light Source, which provide spatial resolution better than 25 nm. Imaging was performed at the Fe L_3 (706 eV) absorption edge, with the sample tilted at 30° to normal incidence to allow the imaging of in-plane magnetic contrast. Magnetic contrast was enhanced either by dividing by reference images taken at saturation, or by differential imaging with right-handed and left-handed polarisation.

We performed initial measurements on both UP and DOWN geometry nanowires with r = 1 μm and g = 160 nm. The nanowires were first saturated into a continuous configuration by applying H_x = - 1 kOe and H_y = ±150 Oe, before H_x = 150-180 Oe was

applied to inject head-to-head (H2H) VDWs from the pads and move them to the notches. The applied field was then removed to relax the VDWs and allow their chiralities to be determined. We then applied H_x = 300-350 Oe to depin the VDWs from the notches and propagate them into the vertical sections of nanowire beyond the corners. The applied field was then removed again to allow the VDWs' final chiralities to be determined.

In Figs. 1(b)-(d) we present example MTXM images that illustrate the results of these measurements. For the UP geometry nanowires VDWs with CW chirality were always observed after the corner no matter whether the injected DWs had CW (Figs. 1(b)) or ACW (Figs. 1(c)) chirality. Conversely for the DOWN geometry nanowires only DWs with ACW chirality were observed after the corner (Figs. 1(d) & 1(e)). Together, these results indicated that the corners had a strong rectifying effect on the chirality of the DWs. The above trends were observed consistently over a total of 28 imaging cycles of the two nanowire geometries, allowing us to reject the hypothesis that the outputted DW was randomly determined at a significance level of 5 %. A total of 8 events were observed where the final chirality of a DW was different from its initial chirality. This allowed us to reject the hypothesis that the probability of the corners transforming DWs with "unfavourable" chiralities was less than 70 % at a significance level of 5 %.

To gain a greater understanding of the chirality rectification process we performed micromagnetic simulations of ACW and CW DWs passing through r = 1 μm corners in UP geometry nanowires using the OOMMF software package [17]. Simulations were performed on a 4 nm x 4 nm x 40 nm 2D mesh using standard parameters to represent the material properties of $Ni_{80}Fe_{20}$: saturation magnetisation, Ms = 860 kA/m, exchange stiffness, A_{ex} =13 pJ/m, magnetocrystalline anisotropy constant, K_1 = 0 and damping constant, α = 0.02. Initial H2H VDW structures were relaxed under zero applied field and then launched ballistically into the corners by applying H_x. Based on the experimental results it was expected that ACW VDWs would be rectified to CW chirality, while CW VDWs would pass through the corner unchanged. To avoid turbulent DW dynamics [7] we performed initial simulations with a low propagation field of H_x = 50 Oe. While this was above the Walker breakdown (WB) field [5], it was within the oscillatory regime of DW motion [6] where dynamics are periodic, and, as we will show later, conserve vortex chirality in this nanowire geometry. Figs. 2(a) & (b) compares the simulated dynamics of DWs with CW and ACW chiralities as they were propagated into the corner. In agreement with the MTXM results, the CW VDW passed into the vertical section of nanowire without changing its chirality, while the ACW VDW was rectified to CW chirality.

Detailed examination of the micromagnetic configurations revealed the underlying cause of the corners' rectifying effect: In the case of the CW VDW the magnetisation in the

leading edge of the VDW pointed along –y, and thus was well-aligned with the magnetisation in the vertical section of nanowire beyond the corner, allowing the it to pass through easily. Conversely, for the ACW DW the magnetisation in the leading edge was along +y, antiparallel to the magnetisation in the vertical section. As the DW approached the corner this resulted in a frustrated and unstable region of magnetisation in front of it, allowing the nucleation of a CW vortex core at 10.2 ns (indicated by a blue arrow in the Fig 2(a)). As the DW moved further around the corner this new CW vortex core moved towards the centre of the nanowire, while the original ACW core moved towards the upper edge of the nanowire, completing the rectification process to a CW VDW.

Figures 2(c) & (d) present equivalent simulations for H_x = 250 Oe, a field closer to that required to depin the DWs from the notches in the experimental measurements. At this higher applied field the dynamics were complex and turbulent, with the DWs becoming extended and containing large numbers of vortex/antivortex cores at any given instant. Nevertheless, the rectification process still occurred, with the extended DWs resolving into CW VDW structure as they passed into the vertical section of nanowire. Clearly, the magnetisation in the vertical section of nanowire was able to bias final nucleation events towards CW chirality as the DWs resolved from unstable structures to stable VDW configurations.

The mechanism we propose above explains why moving from the UP to the DOWN geometry nanowires caused rectification to ACW rather than CW chirality (Figs 1(d) & (e)): in the DOWN geometry the vertical section of nanowire was magnetised along +y rather than –y, and thus would align with leading edge of a ACW VDW, causing rectification to that chirality. Following this logic, one would also expect that changing from H2H to T2T DWs would also switch the nature of the rectification. This is demonstrated for an UP geometry nanowire in Fig. 1(f) where we present MTXM images showing a T2T CW VDW being rectified to ACW chirality rather than maintaining its CW chirality as would have occurred for a H2H VDW.

To probe how the rectification process depended on the geometries of the corners and the fields at which the DWs encountered them we performed further simulations with a range of corner radii and propagation fields. For corners with r > 2 μm we used the graphics processing unit accelerated Mumax[3] software package [18] rather than OOMMF to decrease computation time. For each value of r simulated we found that there was a critical field, H_R, below which the rectification process was suppressed. Data presenting H_R as a function of r is presented in Fig. 3(a). For the larger corner radii simulated we found the value of H_R to be poorly defined, with rectification occurring sporadically over a range of fields (marked with open symbols in the figure). In these geometries, we suggest that the rectification process was sensitive to the magnetisation configuration of the DW, in addition to the magnitude of the

applied field. As the DWs were propagating above WB in all of the simulations presented, slight variations in their structures at the point of encountering the corners would be expected. However, despite these complexities the data still clearly showed H_R to increase with r.

To test the predictions of the simulations we performed imaging of two further structures: an UP geometry nanowire with r = 2 μm and g = 160 nm, and a DOWN geometry nanowire with r = 5 μm and no notch. In the r = 2 μm device we found that all VDWs rectified to CW chirality, as would be expected given that H_x = 250-300 Oe was required to depin the VDWs from the notch. In the r = 5 μm device, DWs propagated directly from the pad to the corner at a lower field of H_x ~180 Oe which, considering the trend in Fig 3(a), was close to the boundary between sporadic and reliable rectification. Indeed, in a total of 19 imaging cycles of this device we observed an instance of a VDW with CW chirality being produced rather than the favoured ACW chirality (Fig. 3(b)), adding evidence to validity of our simulations.

Thus far we have focused on the reliability of the rectification process, however for applications where data is encoded using the chirality of VDWs [11] it would be necessary to to propagate DWs around corners without chirality modification. Fig. 3(a) indicates that for $Ni_{80}Fe_{20}$ this would only be possible at H_x <50 Oe unless the corners had very high radii. However, the damping constant of $Ni_{80}Fe_{20}$ can be enhanced to α = 0.3 - 0.8 by doping with rare earth elements [19,20], causing DWs propagate more rigidly [21] and thus be less susceptible to chirality modification. Fig 3(a) also presents data showing the variation of H_R with r for α = 0.5. With enhanced damping H_R > 100 Oe even for corners with r < 1 μm. Thus, modifying damping provides a route to stabilising chirality-encoded information in complex nanowire networks.

Having shown the ability of corners to rectify the chiralities of VDWs we turned our attention to demonstrating their functionality in device designs. It is well known that DWs pinned at artificial defect sites exhibit stochastic, multi-mode depinning field distributions, due to DWs pinning in a variety of configurations. These configurations can consist of DWs with different internal magnetisation structures (i.e. transverse (TDW) or vortex) [22] or, in the case of asymmetric defect sites, with different chiralities [8,9]. Choosing nanowire geometries that strongly favour TDWs or VDWs should prevent structural variations, however eliminating chirality dependent effects is more challenging, requiring both control of the initial chiralities of the DWs and WB modes that conserve chirality.

Fig. 4(a) presents a simulation of a ACW VDW propagating under H_x = 50 Oe. The dynamics consisted of periodic elongations and contractions of the DW, with multiple vortices and anti-vortices forming along its central boundary during the elongation phase. Critically, the basic symmetry of the DW was maintained at all times so that its chirality was

always conserved on contracting back to VDW structure. Furthermore, micromagnetic simulations indicated that the energy of a bi-domain state containing a TDW was 26 % higher than one containing a VDW making the pinning of TDWs at defect sites highly unlikely. Therefore, it was expected that by combining this nanowire geometry with our technique for regulating DW chirality it should be possible to supress the stochasticity of VDW pinning at asymmetric depinning sites.

To demonstrate this we fabricated nanowires with the geometries labelled “Straight”, “Above” and “Below” in Figs. 4(b)-(d). Each nanowire contained a 60 nm deep triangular notch placed in the top edge of the horizontal section of nanowire, where the stochasticity of DW pinning could be probed. In the “Above” and “Below” nanowire designs we added r = 1 μm corners to rectify the chiralities of VDWs injected from the nucleation pads. Based on our previous results we expected that T2T VDWs in the “Above” devices would rectify to ACW chirality, while those in the “Below” geometry would rectify to CW chirality. We characterised the nanowires’ switching using a focused magneto-optic Kerr effect magnetometer with a spot size of ~4 μm. DW injection and depinning field distributions were measured by performing 100 single shot measurements at the locations labelled “injection” and “depinning” in Fig. 4.

Fig 4(b) shows data obtained from a “Straight” geometry nanowire, where a mixture of CW and ACW DWs were expected to pin at the notch. The depinning field distribution showed high degree of stochasticity with two clear peaks separated by ~170 Oe. Based on the results of micromagnetic simulations of VDW depinning fields for the chosen notch geometry we assigned the peak at the lower field to ACW VDWs and the peak at the higher field to CW VDWs. Figs. 4(c) & (d) present the results of equivalent measurements on the “Above” and “Below” geometry nanowires. Both nanowires exhibited depinning field distributions with only a single peak, corresponding to the expected ACW VDWs for the “Above” geometry and CW VDWs for the “Below” geometry. We also performed similar measurements on two further devices of each geometry. Across three “Straight” geometry nanowires we observed a relatively even split between depinning events assigned to ACW and CW VDWs (4.5 % to 55 %). For the “Above” nanowires we observed a strong bias towards ACW VDWs (84 % ACW to 16 % CW), while for the “Below” nanowires we observed the opposite trend (94 % CW to 6 % ACW). Cumulatively, these results indicate the feasibility of using nanowire corners to supress stochastic pinning behaviour.

In summary, we have shown that the chiralities of VDWs in planar magnetic nanowires are rectified when they are propagated ballistically into tight nanowire corners, with the sense of rectification being determined by whether the nanowires turn left or right. In contrast to previously demonstrated methods of controlling the chirality of propagating DWs

[13-15] this approach can be implemented in continuous nanowires, and does not require the inclusion of strong defect sites. Rectification can be supressed by increasing the radii of nanowire corners, propagating VDWs at low fields, or by increasing the damping constant of the material from which the nanowires are patterned. We have also demonstrated how our approach can be combined with modes of DW propagation that conserve vortex chirality to dramatically reduce the stochasticity of DW pinning at artificial defect sites.

In addition to providing a simple tool to gain control over VDW chirality in further experimental studies we anticipate that our results will find utility in the design of chirality-based logic devices [11] where the chiralities of VDWs must controllably switched as they propagate through complex nanowire networks. Furthermore, corners could be used to "reset" the chirality of propagating VDWs in order to supress stochastic pinning effects in more conventional devices where data is encoded using the orientation of magnetic domains.

This work was supported by the EPSRC (grant EP/J002275/1). The operation of the microscope was supported by the Director, Office of Science, Office of Basic Energy Sciences, Materials Sciences and Engineering Division, of the U.S. Department of Energy under Contract No. DE-AC02-05-CH11231.P.F. and M.-Y.I. acknowledge support by the Leading Foreign Research Institute Recruitment Program (Grant No. 2012K1A4A3053565) through the National Research Foundation of Korea (NRF) funded by the Ministry of Education, Science and Technology (MEST).

[1] G. Hrkac, J. Dean and D.A. Allwood, Philosophical Transactions of the Royal Society A – Mathematical Physical and Engineering Sciences **369**, 3214 (2011).

[2] S.S.P. Parkin, M. Hayashi, and L. Thomas, *Science,* **320**, 190-194, (2008).

[3] D. A. Allwood, G. Xiong, C. C. Faulkner, D. Atkinson, D. Petit, and R. P. Cowburn, Science, 309, 1688 (2005).

[4] R. D. McMichael and M. J. Donahue, IEEE. Trans. Magn. **33**, 4167 (1997).

[5] N.L. Schryer and L.R. Walker, J. Appl. Phys. **45**, 5406 (1974).

[6] J.-Y. Lee, K.-S. Lee, S. Choi, K.Y. Guslienko and S.-R. Kim, Phys. Rev. B **76**, 184408 (2007).

[7] S.-K. Kim, J.-Y. Lee, Y.-S. Choi, K.Y. Guslienko and K.-S. Lee, Appl. Phys. Lett. **93**, 052503 (2008).

[8] M. Hayashi, L. Thomas, C. Rettner, R. Moriya, X. Jiang and S.S.P. Parkin, Phys. Rev. Lett. **97**, 207205 (2006).

[9] L.K. Bogart, D. Atkinson, K. O'Shea, D. McGrouther and S. McVitie, Phys. Rev. B. **79**, 054414 (2009).

[10] A. Pushp, T. Phung, C. Rettner, B.P. Hughes, S.-H. Yang, L. Thomas and S.S.P. Parkin *et. al.,* Nature Phys. **9**, 505 (2013).

[11] K.A. Omari and T.J. Hayward, Phys. Rev. Appl. **2**, 044001 (2014).

[12] D. McGrouther, S. McVitie, J.N. Chapman and A. Gentils, Appl. Phys. Lett. **91**, 022506 (2007).

[13] E.R. Lewis, D. Petit, L. O'Brien, A. Fernandez-Pacheco and J. Sampaio, A.V. Jausovec, H.T. Zeng, D.E. Read and R.P. Cowburn, Nature Physics **9**, 980 (2010).

[14] J. Brandão, R.L. Novak, H. Lozano, P.R. Soledade, A. Mello, F. Garcia and L.C. Sampaio, J. Appl. Phys. **116**, 193902 (2014).

[15] E.-S. Wilhelm, D. McGrouther, L. Heyne, A. Bisig and M. Kläui, Appl. Phys. Lett. **95**, 252501 (2009).

[16] A. Bisig, M.-A. Mawass, M. Stärk, C. Moutafis, J. Rhensius, J. Heidler, S. Gliga, M. Weigand, T. Tyliszczak, B. Van Waeyenberge, H. Stoll, G. Schütz and M. Kläui, Appl. Phys. Lett. **106**, 122401 (2015).

[17] Object Orientated Micromagnetic Framework (OOMMF)
http://math.nist.gov/oommf/

[18] A. Vansteenkiste, J. Leliaert, M. Dvornik, F. Garcia-Sanchez and B. Van Waeyenberge, AIP Advances **4**, 107133 (2014).

[19] G. Woltersdorf, M. Kiessling, G. Meyer, J. U. Thiele, and C. H. Back, Phys. Rev. Lett. **102**, 257602 (2009).

[20] W. Bailey, P. Kabos, F. Mancoff, and S. Russek, IEEE Trans. Magn. **37**, 1749 (2001).

[21] T.A. Moore, P. Mohrke, L. Heyne, A. Kaldun, M. Kläui, D. Backes, J. Rhensius, L.J. Heyderman, J.U. Thiele, G. Woltersdorf, A.F. Rodriguez, F. Nolting, T.O. Mentes, M.A. Nino, A. Locatelli, A. Potenza, H. Marchetto, S. Cavill and S.S. Dhesi, Phys. Rev. B. **82**, 094445 (2010).

[22] M.-Y. Im, L. Bocklage, P. Fischer and G. Meier, Phys. Rev. Lett. **102**, 147204 (2009).

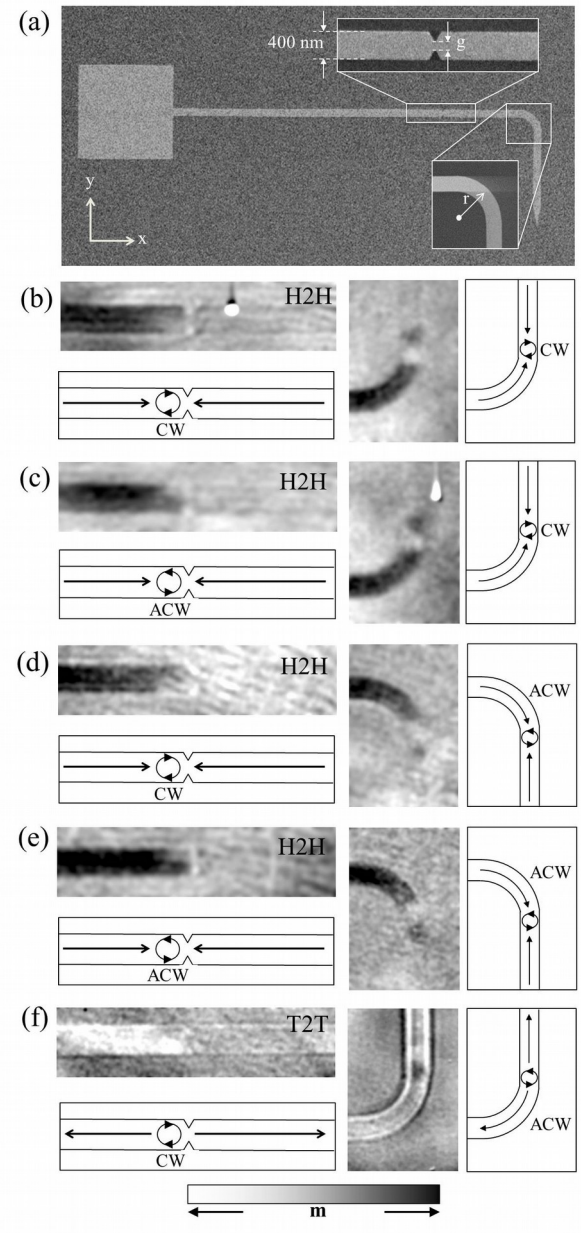

Fig 1: (a) Scanning electron microscope image of a “DOWN” geometry nanowire. Enlargements of the notch and corner regions at which MTXM images were taken are shown inset. (b)-(f) MTXM images showing domain wall configurations before and after passing through the corners: (b) UP geometry nanowire with CW H2H VDW input. (c) UP geometry nanowire with ACW H2H VDW input. (d) DOWN geometry nanowire with CW H2H VDW input. (e) DOWN geometry nanowire with ACW H2H VDW input. (f) UP geometry nanowire with CW T2T VDW input.

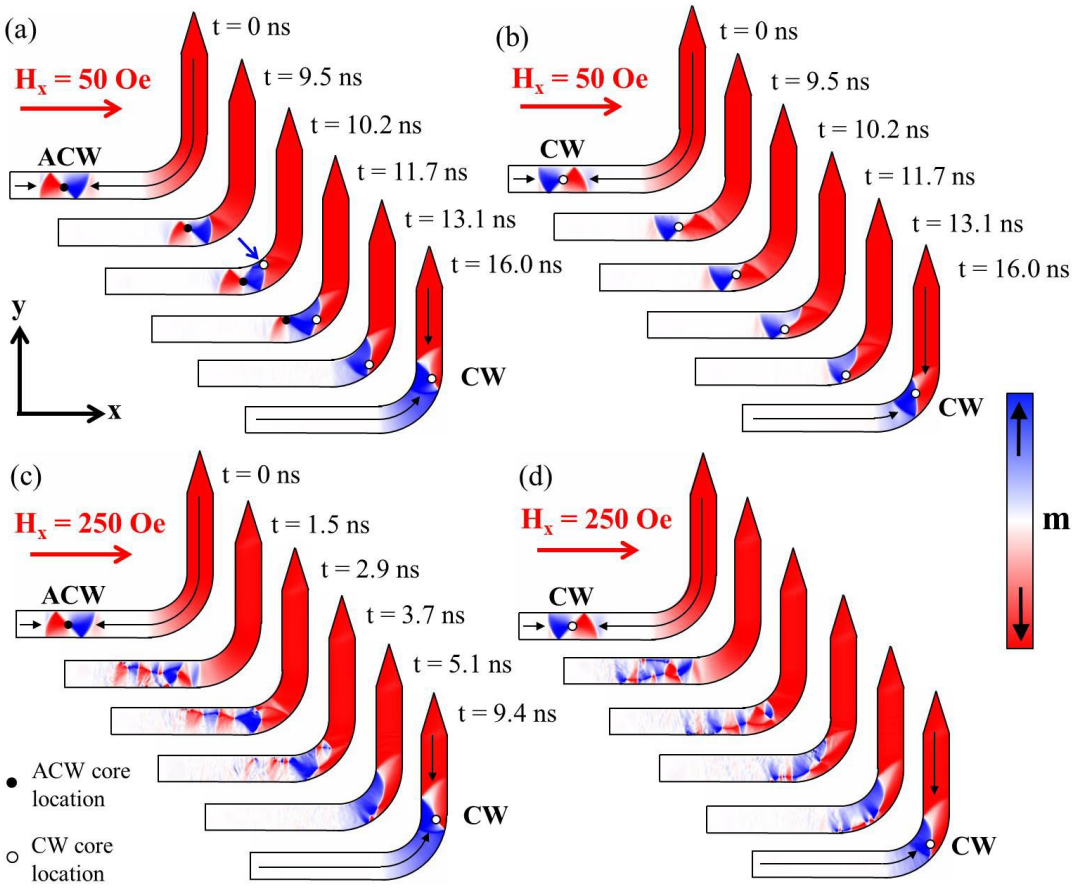

Fig 2: Micromagnetic simulations of VDWs passing through corners with r = 1 μm in a 400 nm wide, 40 nm thick $Ni_{80}Fe_{20}$ nanowire. (a) H_x = 50 Oe, ACW initial VDW chirality. (b) H_x = 50 Oe, CW initial VDW chirality. (c) H_x = 250 Oe, ACW initial VDW chirality. (d) H_x = 250 Oe, CW initial VDW chirality. The locations of the cores of CW and ACW vortices are identified with open and closed symbol respectively, except in the intermediate images of (c) & (d) where the magnetisation dynamics are highly turbulent.

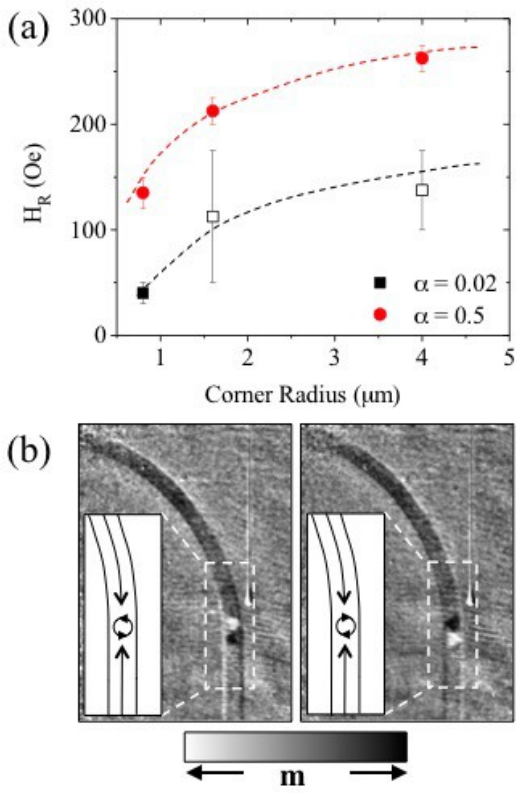

Fig 3: (a) Plot showing the simulated field required to rectify VDWs (H_R) as a function of corner radius for 375 nm wide, 40 nm thick $Ni_{80}Fe_{20}$. Data is shown for damping constants α = 0.02 (squares) and α = 0.5 (circles). Where open symbols are used the error bars indicate a field range over which rectification was seen sporadically. (b) MTXM images showing ACWand CW VDW configurations formed after the corner of a “DOWN” geometry nanowire with r = 5 μm and no notch.

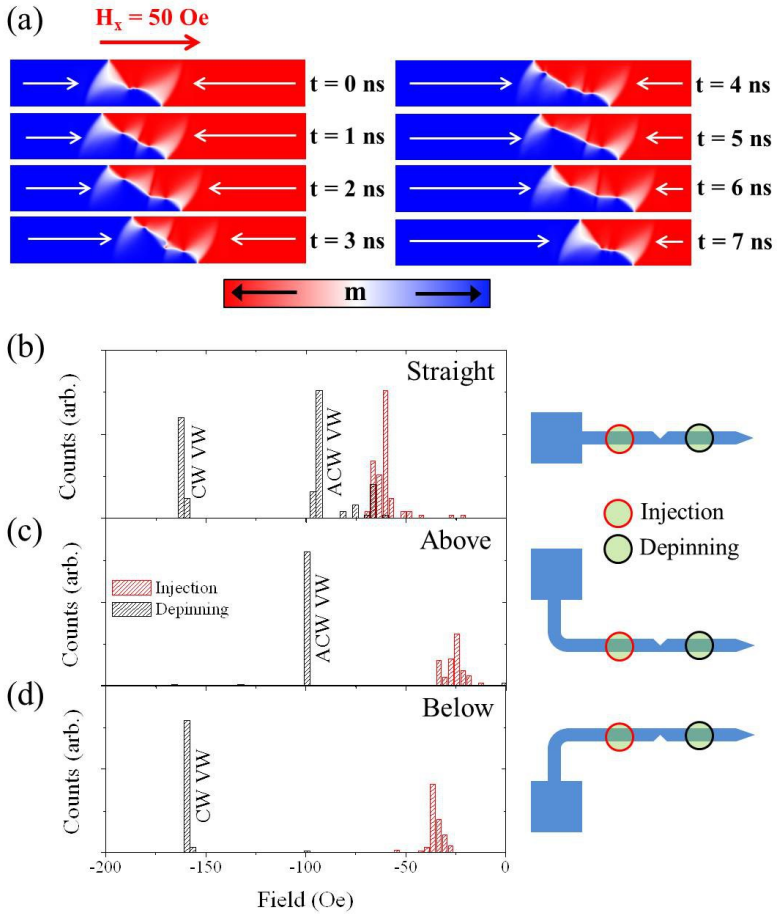

Fig. 4: (a) Simulated VDW dynamics at H_x = 50 Oe in a 400 nm wide, 40 nm thick $Ni_{80}Fe_{20}$ nanowire. The images show a full period of the Walker breakdown oscillations. (b)-(d) Injection and depinning field distributions measured for (a) "Straight", (b) "Above" and (d) "Below" geometry nanowires. The schematic diagrams on the left of the figures indicate the positions of the laser spot for the injection and depinning field measurements.